SCIENCE AND TECHNOLOGY ORGANIZATION
CENTRE FOR MARITIME RESEARCH AND EXPERIMENTATION

Reprint Series CMRE-PR-2019-057

Multiple sensor measurement updates for the extended target tracking random matrix model

Gemine Vivone, Karl Granström, Paolo Braca, Peter Willett

June 2019

Originally published in:

IEEE Transactions on Aerospace and Electronic Systems, volume 53, issue 5, October 2017, pp. 2544-2558, doi: 10.1109/TAES.2017.2704166

About CMRE

The Centre for Maritime Research and Experimentation (CMRE) is a world-class NATO scientific research and experimentation facility located in La Spezia, Italy.

The CMRE was established by the North Atlantic Council on 1 July 2012 as part of the NATO Science & Technology Organization. The CMRE and its predecessors have served NATO for over 50 years as the SACLANT Anti-Submarine Warfare Centre, SACLANT Undersea Research Centre, NATO Undersea Research Centre (NURC) and now as part of the Science & Technology Organization.

CMRE conducts state-of-the-art scientific research and experimentation ranging from concept development to prototype demonstration in an operational environment and has produced leaders in ocean science, modelling and simulation, acoustics and other disciplines, as well as producing critical results and understanding that have been built into the operational concepts of NATO and the nations.

CMRE conducts hands-on scientific and engineering research for the direct benefit of its NATO Customers. It operates two research vessels that enable science and technology solutions to be explored and exploited at sea. The largest of these vessels, the NRV Alliance, is a global class vessel that is acoustically extremely quiet.

CMRE is a leading example of enabling nations to work more effectively and efficiently together by prioritizing national needs, focusing on research and technology challenges, both in and out of the maritime environment, through the collective Power of its world-class scientists, engineers, and specialized laboratories in collaboration with the many partners in and out of the scientific domain.

Copyright © IEEE, 2017. NATO member nations have unlimited rights to use, modify, reproduce, release, perform, display or disclose these materials, and to authorize others to do so for government purposes. Any reproductions marked with this legend must also reproduce these markings. All other rights and uses except those permitted by copyright law are reserved by the copyright owner.

NOTE: The CMRE Reprint series reprints papers and articles published by CMRE authors in the open literature as an effort to widely disseminate CMRE products. Users are encouraged to cite the original article where possible.

Multiple Sensor Measurement Updates for the Extended Target Tracking Random Matrix Model

GEMINE VIVONE
University of Salerno, Fisciano, Italy

KARL GRANSTRÖM, Member, IEEE
Chalmers University of Technology, Gothenburg, Sweden

PAOLO BRACA, Senior Member, IEEE
North Atlantic Treaty Organization Science and Technology Organization Centre for Maritime Research and Experimentation, La Spezia, Italy

PETER WILLETT, Fellow, IEEE
University of Connecticut, Storrs, CT, USA

In this paper, multiple sensor measurement update is studied for a random matrix model. Four different updates are presented and evaluated: three updates based on parametric approximations of the extended target state probability density function and one update based on a Rao–Blackwellized (RB) particle approximation of the state density. An extensive simulation study shows that the RB particle approach shows best performance, at the price of higher computational cost, compared to parametric approximations.

Manuscript received April 19, 2017; revised April 22, 2017; released for publication May 4, 2017. Date of publication May 17, 2017; date of current version October 10, 2017.

DOI. No. 10.1109/TAES.2017.2704166

Refereeing of this contribution was handled by M. Efe.

The work of G. Vivone and P. Braca was supported by the NATO Supreme Allied Command Transformation under Project SAC000608.

Authors' addresses: G. Vivone is with the Department of Information Engineering, Electrical Engineering and Applied Mathematics, University of Salerno, Fisciano 84084, Italy, E-mail: (gvivone@unisa.it); K. Granström is with the Department of Signals and Systems, Chalmers University of Technology, Gothenburg 412 96, Sweden, E-mail: (karl.granstrom@chalmers.se); P. Braca is with the North Atlantic Treaty Organization Science and Technology Organization Centre for Maritime Research and Experimentation, La Spezia 19126, Italy, E-mail: (paolo.braca@cmre.nato.int); P. Willett is with the Department of Electrical and Computer Engineering, University of Connecticut, Storrs, CT 06269-2157, USA, E-mail: (willett@engr.uconn.edu). *(Corresponding author: Gemine Vivone.)*

0018-9251 © 2017 IEEE

I. INTRODUCTION

Very high resolution radars are becoming technologies of great interest. These systems are able to acquire more than one detection for each target per frame. The tracking literature is replete with approaches that make the hypothesis of at most one detection per target, see for instance [1]–[4]. However, in recent years some target tracking researchers have removed that hypothesis: This is *extended target tracking* (ETT). A tutorial introduction to ETT is given in [5].

The literature contains several different approaches to the ETT problem. By using clustering and centroid extraction on the data in a preprocessing step, the processed data can be fed into a point target tracking algorithm [1]. Dedicated ETT algorithms avoid such preprocessing and instead work directly on the sets of detections. Typically, the measurement process is modeled by a cardinality distribution and a spatial density. The cardinality distribution models the number of detections from a target, and the Poisson distribution is a common choice [6], [7]. The spatial density models how the measurements are distributed around the target.

Spatial density models are used for estimating both kinematic parameters and shape parameters of extended targets. There are several different spatial density models in the literature, e.g., the random matrix model [8], [9], the random hypersurface model [10], and models based on Gaussian processes [11]–[13]. Introductions to these models can be found in [5]. In this paper, we use the random matrix model, which to date is one of the more common spatial density models.

The random matrix model is based on the assumption that the target's shape can be approximated by an ellipse, and the spatial spread of the detections can be modeled by a Gaussian distribution whose covariance is proportional to target's elliptic extent. Several improvements and extensions of the original random matrix model [8] have been presented, e.g., improved measurement noise modeling [9], [14], improved motion modeling [15], and tracking under kinematic constraints [16]. Further, the random matrix model has been extended to modeling of nonellipsoidal targets based on representing the target's shape by a combination of ellipses [17], [18]. The random matrix model is applied to tracking of multiple sea vessels, ranging from large ships to smaller boats, using marine X-band radar data in [19]. The problem of conversion of polar/bistatic data to Cartesian coordinates within the random matrix model is addressed and tested on real data in [20] and [21]. The random matrix model has also been integrated into multiple ETT frameworks, e.g., probability hypothesis density (PHD) filter [22]–[24], cardinalized PHD (CPHD) filter [25], generalized labeled multi-Bernoulli (GLMB) filter and labeled multi-Bernoulli (LMB) filter [26], [27], Poisson multi-Bernoulli mixture (PMBM) filter [28], or probabilistic multihypothesis tracking (PMHT) filter [29], [30].

All of the above-mentioned references consider a single sensor (SS); in this paper, we deal with data from a

network of multiple sensors and focus on the spatial density modeling. The multiple sensor extension is by no means straightforward: The extent of the target differs when it is observed from different perspectives. The scope of this paper is limited by the assumption that there are no clutter measurements and there is exactly one target present in the surveillance area, see also [8] and [9]. Four different multisensor (MS) measurement updates are presented; three updates based on a parametric density representation of the extended target state distribution, and one update based on a Rao–Blackwellized (RB) particle representation of the extended target state distribution. The updates are evaluated and compared in an extensive simulation study using two kinds of simulators evaluating the performance varying the numbers of particles, the numbers of detections per target, the numbers of sensors, and the noise levels. Results show that the RB particle filter gives best results at the price of higher computational cost.

This paper extends the preliminary work [31] by adding the following:

1) Extended descriptions of the four updates;
2) An analysis of the differences and similarities between the three updates based on a Gaussian-inverse Wishart (GIW) extended target state probability density function (pdf);
3) An evaluation of the performance for different numbers of sensors and numbers of detections per sensor;
4) An evaluation of the performance for different measurement noise levels.

Furthermore, in [21], a closed-form solution for fusing MS radar data into the random matrix framework has already been proposed by the authors. In this paper, other three MS approaches (two based on a parametric density representation of the extended target state distribution and one relied upon an RB particle representation of the extended target state distribution) are proposed and compared, in an extensive simulation study, with the approach in [21], here called *fusion approximation* (FA).

Some notations that are used throughout this paper is listed in Table I. This paper is organized as follows. Problem formulation is given in Section II. The main contribution, i.e., the four multiple sensor updates, is presented in Section III. For completeness, extended target prediction is reviewed in Section IV. Results from an extensive numerical simulation study are presented in Section V. Conclusions and future developments are drawn in Section VI. Finally, Appendix A reviews the SS updates, whereas Appendix B details the derivations for the two proposed approaches based on a parametric density representation of the extended target state distribution.

II. PROBLEM FORMULATION

Consider a multistatic radar system that consists of S sensors that acquire data within the same surveillance area. Consider also that all the acquired measurements from the S sensors are converted into a common Cartesian space. The

TABLE I
Notations

- $\mathbb{R}^n$ is the set of real column vectors of length n, $\mathbb{S}^n_{++}$ is the set of symmetric positive definite $n \times n$ matrices, and $\mathbb{N}$ is the set of nonnegative integers.
- $\mathcal{N}(\mathbf{x}; \mathbf{m}, P)$ denotes a multivariate Gaussian pdf over the vector $\mathbf{x} \in \mathbb{R}^{n_x}$ with mean vector $\mathbf{m} \in \mathbb{R}^{n_x}$, and covariance matrix $P \in \mathbb{S}^{n_x}_{++}$.
- $\mathcal{IW}_d(X; v, V)$ denotes an inverse Wishart pdf over the matrix $X \in \mathbb{S}^d_{++}$ with scalar degrees of freedom $v > 2d$ and parameter matrix $V \in \mathbb{S}^d_{++}$, see, e.g., [32, Definition 3.4.1]

$$\mathcal{IW}_d(X; v, V) = \frac{2^{-\frac{v-d-1}{2}} \det(V)^{\frac{v-d-1}{2}}}{\Gamma_d\left(\frac{v-d-1}{2}\right) \det(X)^{\frac{v}{2}}} \operatorname{etr}\left(-\frac{1}{2} X^{-1} V\right) \tag{1}$$

where $\operatorname{etr}(\cdot) = \exp(\operatorname{tr}(\cdot))$ is exponential of the matrix trace indicated by $\operatorname{tr}(\cdot)$, $\det(\cdot)$ is the determinant operator, and $\Gamma_d(\cdot)$ is the multivariate gamma function. The multivariate gamma function $\Gamma_d(\cdot)$ can be expressed as a product of the ordinary gamma function $\Gamma(\cdot)$, see [32, Th. 1.4.1].
- $\mathcal{W}_d(X; w, W)$ denotes a Wishart pdf over the matrix $X \in \mathbb{S}^d_{++}$ with scalar degrees of freedom $w \geq d$ and parameter matrix $W \in \mathbb{S}^d_{++}$, see, e.g., [32, Definition 3.2.1]

$$\mathcal{W}_d(X; w, W) = \frac{2^{-\frac{wd}{2}} \det(X)^{\frac{w-d-1}{2}}}{\Gamma_d\left(\frac{w}{2}\right) \det(W)^{\frac{w}{2}}} \operatorname{etr}\left(-\frac{1}{2} W^{-1} X\right). \tag{2}$$

- Expected prior extent $\hat{X}_{k|k-1}$ [32]

$$\hat{X}_{k|k-1} = \frac{V_{k|k-1}}{v_{k|k-1} - 2d - 2} \tag{3}$$

where $V_{k|k-1}$ is the predicted scale matrix and $v_{k|k-1}$ are the predicted degrees of freedom.
- Expected added effect of the expected prior extent $\hat{X}_{k|k-1}$ and sensor noise represented by the covariance matrix for the sth sensor's measurement noise at time k, i.e., R^s_k, normalized by number of detections n^s_k

$$\hat{Y}^s_{k|k-1} = \frac{\rho \hat{X}_{k|k-1} + R^s_k}{n^s_k} \tag{4}$$

where ρ is a scaling factor.
- Centroid measurement $\bar{\mathbf{z}}^s_k$ and measurement spread Z^s_k for sth sensor are

$$\bar{\mathbf{z}}^s_k = \frac{1}{n^s_k} \sum_{j=1}^{n^s_k} \mathbf{z}^{s,j}_k; \qquad Z^s_k = \sum_{j=1}^{n^s_k} \left(\mathbf{z}^{s,j}_k - \bar{\mathbf{z}}^s_k\right)\left(\mathbf{z}^{s,j}_k - \bar{\mathbf{z}}^s_k\right)^{\mathrm{T}} \tag{5}$$

where $\mathbf{z}^{s,j}_k$ is the jth measurement for the sth sensor at time k and $(\cdot)^{\mathrm{T}}$ is the transpose operator. Note: measurement spread is not equivalent to sample covariance.
- Cholesky factorization of positive definite matrix A is denoted

$$A = \left(A^{\frac{1}{2}}\right)^{\mathrm{T}} A^{\frac{1}{2}} = A^{\frac{\mathrm{T}}{2}} A^{\frac{1}{2}}. \tag{6}$$

For brevity, we denote the transpose of the upper triangular matrix $A^{\frac{1}{2}}$ by $A^{\frac{\mathrm{T}}{2}}$.
- Delta function for $\mathcal{X}^d$, space of all $d \times d$ matrices

$$\delta(X) = 0 \text{ if } X \neq \mathbf{0}^d, \text{ for } X \in \mathcal{X}^d \tag{7}$$

$$\int_{\mathcal{X}} \delta(X) \mathrm{d}X = 1 \tag{8}$$

where $\mathbf{0}^d$ is a $d \times d$ all-zero-matrix. For brevity, we use the following notation $\delta_X(Y) = \delta(X - Y)$.

conversion is taken into account, thanks to proper noise covariance matrices [20], [21]. Inside the surveillance area, an extended target is located. The extended target state is modeled by a kinematic vector $\mathbf{x}_k$ and an extent matrix X_k. The kinematic vector describes the target's position as well as motion parameters such as velocity and turn-rate. The extent matrix describes the target's spatial extent, under an assumption that the shape is approximated by an ellipse.

The set of target measurements acquired at time k by the sth sensor is denoted as

$$\mathbf{Z}_k^s = \left\{\mathbf{z}_k^{s,j}\right\}_{j=1}^{n_k^s} \tag{9}$$

where $\mathbf{z}_k^{s,j}$ are the measurements and n_k^s is the number of measurement for the sth sensor at time k. The detections $\mathbf{z}_k^{s,j}$ for the sth sensor at time k are assumed independent and each sensor s acquires n_k^s measurements of the target at time k. The full set of detections at time k is the union of the sets of detections from the $S \in \mathbb{N}$ sensors

$$\mathbf{Z}_k^c = \bigcup_{s=1}^{S} \mathbf{Z}_k^s. \tag{10}$$

Let $\mathbf{Z}^{c,k} = \left\{\mathbf{Z}_\ell^c\right\}_{\ell=0}^{k}$ denotes all such measurement sets up to, and including, time k.

The problem considered in this paper is that of MS measurement update, i.e., given a prior distribution for the extended target state

$$p(\mathbf{x}_k, X_k|\mathbf{Z}^{c,k-1}) \tag{11a}$$

find the posterior distribution

$$p(\mathbf{x}_k, X_k|\mathbf{Z}^{c,k}). \tag{11b}$$

This is achieved using the Bayes' update

$$p(\mathbf{x}_k, X_k|\mathbf{Z}^{c,k}) = \frac{p\left(\mathbf{Z}_k^c|\mathbf{x}_k, X_k\right) p(\mathbf{x}_k, X_k|\mathbf{Z}^{c,k-1})}{\iint p\left(\mathbf{Z}_k^c|\mathbf{x}_k, X_k\right) p(\mathbf{x}_k, X_k|\mathbf{Z}^{c,k-1})\,\mathrm{d}\mathbf{x}_k\mathrm{d}X_k} \tag{12}$$

where

$$p\left(\mathbf{Z}_k^c|\mathbf{x}_k, X_k\right) = p\left(\mathbf{Z}_k^c\middle|\mathbf{x}_k, X_k, \left\{n_k^s\right\}_{s=1}^{S}\right) p\left(\left\{n_k^s\right\}_{s=1}^{S}\middle|\mathbf{x}_k, X_k\right) \tag{13}$$

is the MS measurement likelihood with cardinality distribution $p(\{n_k^s\}_{s=1}^S|\mathbf{x}_k, X_k)$ and spatial density $p(\mathbf{Z}_k^c|\mathbf{x}_k, X_k, \{n_k^s\}_{s=1}^S)$. This likelihood describes, for a target with state $\mathbf{x}_k$, X_k, how many detections the sensors will give, and how the detections are distributed spatially around the target. Modeling the cardinality distribution and estimating the number of detections is outside the scope of this paper; we refer the readers to the literature, e.g., [6], [7], and [33].

The MS measurement likelihood, conditioned on the extended target state $\mathbf{x}_k$, X_k and the number of detections n_k^s, i.e., the spatial density, is here modeled as

$$p\left(\mathbf{Z}_k^c\middle|\mathbf{x}_k, X_k, \left\{n_k^s\right\}_{s=1}^{S}\right) = \prod_{s=1}^{S}\prod_{j=1}^{n_k^s} \mathcal{N}\left(\mathbf{z}_k^{s,j};\, H_k\mathbf{x}_k, \rho X_k + R_k^s\right) \tag{14}$$

where H_k is a measurement model at time k that selects the position components in the state vector, ρ is a scaling factor, and R_k^s is a covariance matrix for the sth sensor's measurement noise at time k. This model can be understood to model the detections as being located on the target's extent and corrupted by Gaussian measurement noise with zero mean and covariance R_k^s.[1]

We consider two different parameterizations of the prior and posterior densities (11): factorized GIW density and RB particle representation.

For Gaussian distributed detections with negligible measurement noise ($R_k^s \approx 0$), the conjugate prior for unknown $\mathbf{x}_k$ and unknown X_k is a GIW distribution [8]

$$p(\mathbf{x}_k, X_k|\mathbf{Z}^{c,k-1}) = p(\mathbf{x}_k|X_k, \mathbf{Z}^{c,k-1})p(X_k|\mathbf{Z}^{c,k-1}) \tag{15a}$$

$$= \mathcal{N}\left(\mathbf{x}_k;\, m_{k|k-1}, P_{k|k-1} \otimes X_k\right) \times \mathcal{IW}_d\left(X_k;\, v_{k|k-1}, V_{k|k-1}\right) \tag{15b}$$

where $m_{k|k-1}$ and $P_{k|k-1}$ are the prior kinematic state estimation and covariance, respectively, $v_{k|k-1}$ and $V_{k|k-1}$ are the prior degrees of freedom and scale matrix, respectively, and $\otimes$ indicates the Kronecker product.

In the SS case, the posterior distribution

$$p(\mathbf{x}_k, X_k|\mathbf{Z}^{c,k}) = p(\mathbf{x}_k|X_k, \mathbf{Z}^{c,k})p(X_k|\mathbf{Z}^{c,k}) \tag{15c}$$

$$= \mathcal{N}\left(\mathbf{x}_k;\, m_{k|k}, P_{k|k} \otimes X_k\right) \times \mathcal{IW}_d\left(X_k;\, v_{k|k}, V_{k|k}\right) \tag{15d}$$

where $m_{k|k}$ and $P_{k|k}$ are the posterior kinematic state estimation and covariance, respectively, and $v_{k|k}$ and $V_{k|k}$ are the posterior degrees of freedom and scale matrix, respectively. The posterior distribution can be computed analytically, see [8].

However, in most scenarios the measurement noise is not negligible [9], and in this case the posterior distribution cannot be computed analytically. Instead approximate methods are necessary. When the measurement noise is nonnegligible, prior work, see, e.g., [9] and [34], has shown that it is beneficial to factorize the prior and posterior

[1] For brevity and notational simplicity, the dependence of the covariances (R_k^s) of the measurement noise on the kinematic state is not explicitly indicated. However, all derivations in this paper are valid also in the case of kinematic state dependent covariance matrices, see [20].

distributions approximately as

$$p(\mathbf{x}_k, X_k|\mathbf{Z}^{c,k-1}) \approx p(\mathbf{x}_k|\mathbf{Z}^{c,k-1})p(X_k|\mathbf{Z}^{c,k-1}) \quad (16a)$$
$$= \mathcal{N}\left(\mathbf{x}_k\,;\, m_{k|k-1}, P_{k|k-1}\right) \times \mathcal{IW}_d\left(X_k\,;\, v_{k|k-1}, V_{k|k-1}\right) \quad (16b)$$
$$p(\mathbf{x}_k, X_k|\mathbf{Z}^{c,k}) \approx p(\mathbf{x}_k|\mathbf{Z}^{c,k})p(X_k|\mathbf{Z}^{c,k}) \quad (16c)$$
$$= \mathcal{N}\left(\mathbf{x}_k\,;\, m_{k|k}, P_{k|k}\right) \times \mathcal{IW}_d\left(X_k\,;\, v_{k|k}, V_{k|k}\right). \quad (16d)$$

For the SS case, the update can no longer be computed analytically. In the literature, there are approximate updates based on, e.g., Cholesky factorization [9], variational Bayesian approximation [14], and linearization of the log likelihood [35].

In this paper, we consider the MS case and compare four different updates. The first three updates are based on factorized GIW approximations (16) of the extended target state distribution that are as follows:

1) An update based on approximate fusion, proposed in [21];
2) A MS generalization of the SS update from [9];
3) A MS generalization of the SS update from [35].

The SS updates [9], [35] are reviewed in Appendix A. The fourth update assumes an RB particle representation of the extended target state distribution, with a Gaussian distribution for the kinematic state and a particle approximation of the extent state distribution

$$p(\mathbf{x}_k, X_k|\mathbf{Z}^{c,k-1}) \approx p(\mathbf{x}_k|\mathbf{Z}^{c,k-1})p(X_k|\mathbf{Z}^{c,k-1}) \quad (17a)$$
$$= \mathcal{N}\left(\mathbf{x}_k\,;\, m_{k|k-1}, P_{k|k-1}\right) \times \sum_{i=1}^{N_p} w_{k|k-1}^{(i)} \delta_{X_k}\left(X_k^{(i)}\right) \quad (17b)$$
$$p(\mathbf{x}_k, X_k|\mathbf{Z}^{c,k}) \approx p(\mathbf{x}_k|\mathbf{Z}^{c,k})p(X_k|\mathbf{Z}^{c,k}) \quad (17c)$$
$$= \mathcal{N}\left(\mathbf{x}_k\,;\, m_{k|k}, P_{k|k}\right) \times \sum_{i=1}^{N_p} w_{k|k}^{(i)} \delta_{X_k}\left(X_k^{(i)}\right) \quad (17d)$$

where $w_{k|k-1}^{(i)}$ and $w_{k|k}^{(i)}$ are the predicted and posterior weights of the particle i, respectively, and Dirac's delta function is defined in Table I.[2]

To summarize, finding the posterior distribution (11b), given the prior (11a) and the likelihood (14), means to do one of the following two points.

[2]It is possible to approximate the full extended target distribution by a particle filter, thereby obtaining a full particle filter solution. However, this drastically increases the size of the state space that must be sampled. Empirically, we have found that the RB particle representation (17) is a better tradeoff between the performance and the computational burden of the algorithm. Other more computationally demanding options include running a Kalman filter for each particle.

1) If a parametric GIW representation is used for the prior distribution, the posterior GIW parameters
$$\left(m_{k|k}, P_{k|k}, v_{k|k}, V_{k|k}\right) \quad (18)$$
are computed, given a set of detections $\mathbf{Z}_k^c$ and the prior GIW parameters.
$$\left(m_{k|k-1}, P_{k|k-1}, v_{k|k-1}, V_{k|k-1}\right) \quad (19)$$
2) If an RB representation is used for the prior distribution, the posterior RB parameters
$$\left(m_{k|k}, P_{k|k}, w_{k|k}^{(i)}, X_{k|k}^{(i)}\right) \quad (20)$$
are computed given a set of detections $\mathbf{Z}_k^c$ and the prior RB parameters
$$\left(m_{k|k-1}, P_{k|k-1}, w_{k|k-1}^{(i)}, X_{k|k-1}^{(i)}\right). \quad (21)$$

In Section III, we present four different MS updates that are valid for $S \in \mathbb{N}$ sensors; for the sake of clarity the SS case ($S = 1$) is reviewed in Appendix A. Analysis of the extended target prediction, i.e., using a motion model to compute the prior $p(\mathbf{x}_k, X_k|\mathbf{Z}^{c,k-1})$, given the posterior $p(\mathbf{x}_k, X_k|\mathbf{Z}^{c,k})$, is outside the scope of this paper. In Section IV, we review the standard prediction.

III. MULTISENSOR UPDATES

This section presents the kinematic state update and four different MS updates. Section III-A gives the kinematic state update, which is the same for all updates. This is followed by the particle update. Section III-C presents the inverse Wishart updates, with a discussion about similarities and differences.

When the random matrix model is used with nonnegligible measurement noise—as is the case in this paper—the posterior extent state distribution can typically not be evaluated in closed form. Different approaches exist for the single-sensor inverse Wishart case, and here these are generalized to multiple sensors. Additionally, an update for a particle approximation of the extent state density is also presented.

A. Gaussian Kinematic State Update

The kinematic state is updated as follows:

$$m_{k|k}^{\text{MS}} = m_{k|k-1} + K_{k|k-1}^c\left(\bar{\mathbf{z}}_{k|k-1}^c - H_k m_{k|k-1}\right) \quad (22a)$$
$$P_{k|k}^{\text{MS}} = P_{k|k-1} - K_{k|k-1}^c H_k P_{k|k-1} \quad (22b)$$

where

$$\hat{Y}_{k|k-1}^c = \left[\sum_{s=1}^{S}\left(\hat{Y}_{k|k-1}^s\right)^{-1}\right]^{-1} \quad (22c)$$
$$S_{k|k-1}^c = H_k P_{k|k-1} H_k^{\mathsf{T}} + \hat{Y}_{k|k-1}^c \quad (22d)$$
$$K_{k|k-1}^c = P_{k|k-1} H_k^{\mathsf{T}}\left(S_{k|k-1}^c\right)^{-1} \quad (22e)$$
$$\bar{\mathbf{z}}_{k|k-1}^c = \hat{Y}_{k|k-1}^c \sum_{s=1}^{S}\left(\hat{Y}_{k|k-1}^s\right)^{-1}\bar{\mathbf{z}}_k^s \quad (22f)$$

and $\bar{\mathbf{z}}_k^s$ and $\hat{Y}_{k|k-1}^s$ are defined in Table I. If $S = 1$, the MS update kinematic state update (22) reduces to the SS update presented in Appendix A-A. The kinematic measurement update equations presented in this section are the same as measurement fusion Method II in [36] when $n_k^s = 1$ for all the S sensors and the extent is known.

B. Inverse Wishart Extent Updates

1) *FFK Generalization:* The MS generalization of the Feldmann, Franken and Koch (FFK) SS update [9] (MSFFK), see Appendix A-B1, is

$$v_{k|k}^{\text{MSFFK}} = v_{k|k-1} + \sum_{s=1}^{S} n_k^s \tag{23a}$$

$$V_{k|k}^{\text{MSFFK}} = V_{k|k-1} + \sum_{s=1}^{S} Z_{k|k-1}^s + L_{k|k-1}^c \tag{23b}$$

where

$$Z_{k|k-1}^s = \hat{X}_{k|k-1}^{\frac{\mathrm{T}}{2}} \left(\hat{Y}_{k|k-1}^s\right)^{-\frac{\mathrm{T}}{2}} Z_k^s \left(\hat{Y}_{k|k-1}^s\right)^{-\frac{1}{2}} \hat{X}_{k|k-1}^{\frac{1}{2}} \tag{23c}$$

$$L_{k|k-1}^c = \hat{X}_{k|k-1}^{\frac{\mathrm{T}}{2}} \left(S_{k|k-1}^c\right)^{-\frac{\mathrm{T}}{2}} N_{k|k-1}^c \left(S_{k|k-1}^c\right)^{-\frac{1}{2}} \hat{X}_{k|k-1}^{\frac{1}{2}} \tag{23d}$$

$$N_{k|k-1}^c = \left(\bar{\mathbf{z}}_{k|k-1}^c - H_k m_{k|k-1}\right)\left(\bar{\mathbf{z}}_{k|k-1}^c - H_k m_{k|k-1}\right)^{\mathrm{T}} \tag{23e}$$

and $\bar{\mathbf{z}}_{k|k-1}^c$ and $S_{k|k-1}^c$ are defined in (22), and $\hat{X}_{k|k-1}$, Z_k^s and $\hat{Y}_{k|k-1}^s$ are defined in Table I. See Appendix B-A for proof details.

2) *ULL Generalization:* The MS generalization of the unbiased log-likelihood linearization (MSULL) SS update [35], see Appendix A-B2, is

$$v_{k|k}^{\text{MSULL}} = v_{k|k-1} + \sum_{s=1}^{S} n_k^s \tag{24a}$$

$$V_{k|k}^{\text{MSULL}} = V_{k|k-1} + \sum_{s=1}^{S} M_{k|k-1}^s \tag{24b}$$

where

$$M_{k|k-1}^s = n_k^s \hat{X}_{k|k-1} + n_k^s \rho \hat{X}_{k|k-1} (C_{k|k-1}^s)^{-1} \times \left(\frac{Z_k^s}{n_k^s} + N_{k|k-1}^s - C_{k|k-1}^s\right)(C_{k|k-1}^s)^{-1} \hat{X}_{k|k-1} \tag{24c}$$

$$N_{k|k-1}^s = \left(\bar{\mathbf{z}}_k^s - H_k m_{k|k-1}\right)\left(\bar{\mathbf{z}}_k^s - H_k m_{k|k-1}\right)^{\mathrm{T}} \tag{24d}$$

$$C_{k|k-1}^s = H_k P_{k|k-1} H_k^{\mathrm{T}} + \rho \hat{X}_{k|k-1} + R_k^s \tag{24e}$$

and $\hat{X}_{k|k-1}$ is defined in Table I. See Appendix B-B for proof details.

3) *Fusion Approximation:* The following update is based on FA and was presented in [21]

$$v_{k|k}^{\text{FA}} = v_{k|k-1} + \sum_{s=1}^{S} n_k^s \tag{25a}$$

$$V_{k|k}^{\text{FA}} = V_{k|k-1} + Z_{k|k-1}^c + L_{k|k-1}^c \tag{25b}$$

where $L_{k|k-1}^c$ was defined in (23d)

$$\Sigma_{k|k-1}^c = \frac{1}{n_k} \sum_{s=1}^{S} n_k^s \left(\rho \hat{X}_{k|k-1} + R_k^s\right) \tag{25c}$$

$$Z_{k|k-1}^c = \hat{X}_{k|k-1}^{\frac{\mathrm{T}}{2}} \left(\Sigma_{k|k-1}^c\right)^{-\frac{\mathrm{T}}{2}} Z_k^c \left(\Sigma_{k|k-1}^c\right)^{-\frac{1}{2}} \hat{X}_{k|k-1}^{\frac{1}{2}} \tag{25d}$$

$$Z_k^c = \sum_{s=1}^{S} \sum_{j=1}^{n_k^s} \left(\mathbf{z}_k^{s,j} - \bar{\mathbf{z}}_k\right)\left(\mathbf{z}_k^{s,j} - \bar{\mathbf{z}}_k\right)^{\mathrm{T}} \tag{25e}$$

$$\bar{\mathbf{z}}_k = \frac{1}{n_k} \sum_{s=1}^{S} \sum_{j=1}^{n_k^s} \mathbf{z}_k^{s,j}. \tag{25f}$$

The total number of measurements is $n_k = \sum_{s=1}^{S} n_k^s$, and $\hat{X}_{k|k-1}$ is defined in Table I.

4) *Discussion:* The following important similarities between the MSULL, MSFFK, and FA updates can be noted.

First, all three updates rely on the assumption that the true extent X_k can be accurately approximated by the predicted extent estimate $\hat{X}_{k|k-1}$. The MSULL update is derived by first linearizing the log likelihood around $(\mathbf{x}_k, X_k) = \left(\hat{\mathbf{x}}_{k|k-1}, \hat{X}_{k|k-1}\right)$, and then modifying to make the update unbiased. The MSFFK and FA updates use Cholesky factorizations to reformulate functions of the extent X_k, followed by zeroth-order Taylor approximations of nonlinear functions of the extent.

For example, using Cholesky factorization, we can write

$$\frac{\rho X_k + R_k^s}{n_k^s} = \left(\frac{\rho X_k + R_k^s}{n_k^s}\right)^{\frac{\mathrm{T}}{2}} \left(\frac{\rho X_k + R_k^s}{n_k^s}\right)^{\frac{1}{2}} \tag{26a}$$

$$= \left(\frac{\rho X_k + R_k^s}{n_k^s}\right)^{\frac{\mathrm{T}}{2}} \left(X_k^{\frac{\mathrm{T}}{2}}\right)^{-1} X_k \left(X_k^{\frac{1}{2}}\right)^{-1} \left(\frac{\rho X_k + R_k^s}{n_k^s}\right)^{\frac{1}{2}}. \tag{26b}$$

Approximating the matrix square-roots using zeroth-order Taylor expansion around $X_k = \hat{X}_{k|k-1}$, we get the approximations $X_k^{\frac{1}{2}} \approx \hat{X}_{k|k-1}^{\frac{1}{2}}$ and

$$\left(\frac{\rho X_k + R_k^s}{n_k^s}\right)^{\frac{1}{2}} \approx \left(\frac{\rho \hat{X}_{k|k-1} + R_k^s}{n_k^s}\right)^{\frac{1}{2}} = \left(\hat{Y}_{k|k-1}^s\right)^{\frac{1}{2}}. \tag{26c}$$

Inserting into (26b) gives the approximation

$$\frac{\rho X_k + R_k^s}{n_k^s} \approx \left(\hat{Y}_{k|k-1}^s\right)^{\frac{\mathrm{T}}{2}} \hat{X}_{k|k-1}^{-\frac{\mathrm{T}}{2}} X_k \hat{X}_{k|k-1}^{-\frac{1}{2}} \left(\hat{Y}_{k|k-1}^s\right)^{\frac{1}{2}} \tag{26d}$$

which is linear in the extent state X_k.

Unless there is accurate prior information about the size of the extended target, initially the assumption that $X_k \approx \hat{X}_{k|k-1}$ could be less accurate, which would affect the estimation performance. However, empirical evidence shows that this inaccuracy is overcome within a few timesteps, and the estimate converges such that the predicted expected value is close to being equal to the true extent matrix.

Second, in all of the updates, the inverse Wishart degrees of freedom is updated in the same way: By adding the total number of detections in the set $\mathbf{Z}_k^c$, see (23a), (24a), and (25a).

Third, all three updates of the inverse Wishart scale matrix add matrices that are related to the measurement spread, and the spread of the centroid measurement around the predicted position. To see this, we first rewrite the MSULL update matrices $M_{k|k-1}^s$ as

$$M_{k|k-1}^s = \widetilde{Z}_{k|k-1}^s + \widetilde{N}_{k|k-1}^s + n_k^s \hat{X}_{k|k-1} - n_k^s \rho \hat{X}_{k|k-1} (C_{k|k-1}^s)^{-1} \hat{X}_{k|k-1} \tag{27a}$$

where

$$\widetilde{Z}_{k|k-1}^s = \rho \hat{X}_{k|k-1} (C_{k|k-1}^s)^{-1} Z_k^s (C_{k|k-1}^s)^{-1} \hat{X}_{k|k-1} \tag{27b}$$

$$\widetilde{N}_{k|k-1}^s = n_k^s \rho \hat{X}_{k|k-1} (C_{k|k-1}^s)^{-1} N_{k|k-1}^s (C_{k|k-1}^s)^{-1} \hat{X}_{k|k-1}. \tag{27c}$$

Note that the MSULL scale matrix update (24b) adds the sum of $M_{k|k-1}^s$ to the predicted scale matrix.

Comparing the three updates, we see that $\sum_{s=1}^S Z_{k|k-1}^s$ in (23b) and $Z_{k|k-1}^c$ in (25b) are analogous to $\sum_{s=1}^S \widetilde{Z}_{k|k-1}^s$, as they describe the spread of the measurements around the centroid measurement. For MSFFK and MSULL, we have sums over the spreads for the individual sensors, whereas FA computes the spread for all measurements from all sensors. Furthermore, we also see that $L_{k|k-1}^c$ in (23b) and (25b) is analogous to $\sum_{s=1}^S \widetilde{N}_{k|k-1}^s$, as they describe the spread of the centroid around the predicted measurement $H_k m_{k|k-1}$. Here, MSFFK and FA describe the spread around the centroid for all sensors, whereas MSULL has a sum of the spreads around the individual sensor centroids.

C. Particle Approximation Extent Update

Assume that at time $k-1$, a set of weighted particles representing the posterior is available

$$\left\{ w_{k-1}^{(i)}, X_{k-1}^{(i)} \right\}_{i=1}^{N_p} \tag{28}$$

$$p\left(X_{k-1} | \mathbf{Z}^{c,k-1}\right) \approx \sum_{i=1}^{N_p} w_{k-1}^{(i)} \delta_{X_{k-1}^{(i)}}(X_{k-1}). \tag{29}$$

The logarithm of the single-sensor likelihood for the sth sensor, see (14), can be approximated as

$$\log\ p\left(\mathbf{Z}_k^s \middle| \mathbf{x}_k, X_k, n_k^s\right) = -\frac{n_k^s}{2} \log\det(\rho X_k + R_k^s) - \frac{1}{2} \sum_{j=1}^{n_k^s} \left(\mathbf{z}_k^{s,j} - H_k \mathbf{x}_k\right)^{\mathsf{T}} (\rho X_k + R_k^s)^{-1} \left(\mathbf{z}_k^{s,j} - H_k \mathbf{x}_k\right) + \text{const.} \tag{30}$$

Similarly to how in the kinematic state update where the extent state is approximated by its predicted expected value [see (4) and (22)], here we approximate the kinematic state by its predicted expected value in order to split the estimation problem into two parts: kinematic and extent. Thus, this approximation avoids to jointly sample both the states (i.e., the extent state and the kinematic state) strongly reducing the computational burden of the proposed approach.

Algorithm 1: Particle Filter Algorithm.

At time $k \geq 1$

- **Sampling Step**
- For $i = 1, \ldots, N_p$, sample $\widetilde{X}_k^{(i)} \sim q\left(\cdot | X_{k-1}^{(i)}, \mathbf{Z}_k^c\right)$, set $\widetilde{w}_k^{(i)} = \mathcal{L}_k\left(\mathbf{Z}_k^c | \widetilde{X}_k^{(i)}\right) w_{k-1}^{(i)}$. (38)
- Normalize weights: $\sum_{i=1}^{N_p} \widetilde{w}_k^{(i)} = 1$.
- **Resampling Step**
- Resample $\left\{\widetilde{w}_k^{(i)}, \widetilde{X}_k^{(i)}\right\}_{i=1}^{N_p}$ to get $\left\{w_k^{(i)}, X_k^{(i)}\right\}_{i=1}^{N_p}$.

Thus, we approximate $\mathbf{x}_k \approx m_{k|k-1}$, and the SS log-likelihood approximation (30) can be rewritten as

$$\log\ p\left(\mathbf{Z}_k^s \middle| \mathbf{x}_k, X_k, n_k^s\right) \approx -\frac{n_k^s}{2} \log\det(\rho X_k + R_k^s) - \frac{1}{2} \mathrm{tr}\left[(\rho X_k + R_k^s)^{-1} \Sigma_k^s\right] + \text{const} \tag{31}$$

where

$$\Sigma_k^s = \sum_{j=1}^{n_k^s} \left(\mathbf{z}_k^{s,j} - H_k m_{k|k-1}\right) \left(\mathbf{z}_k^{s,j} - H_k m_{k|k-1}\right)^{\mathsf{T}} \tag{32}$$

$$= Z_k^s + n_k^s (\bar{\mathbf{z}}_k^s - H_k m_{k|k-1})(\bar{\mathbf{z}}_k^s - H_k m_{k|k-1})^{\mathsf{T}}. \tag{33}$$

The logarithm of the MS likelihood (14) is the sum of the SS log likelihoods

$$\log\ p\left(\mathbf{Z}_k^c \middle| \mathbf{x}_k, X_k, \{n_k^s\}_{s=1}^S\right) = \sum_{s=1}^S \log p\left(\mathbf{Z}_k^s \middle| \mathbf{x}_k, X_k, n_k^s\right) \tag{34}$$

$$\approx -\frac{1}{2} \sum_{s=1}^S \left\{ n_k^s \log\det(\rho X_k + R_k^s) + \mathrm{tr}\left[(\rho X_k + R_k^s)^{-1} \Sigma_k^s\right] \right\} + \text{const.} \tag{35}$$

$$= \log\ \mathcal{L}_k(\mathbf{Z}_k^c | X_k) \tag{36}$$

where $\mathcal{L}_k(\mathbf{Z}_k^c | X_k)$ is shorthand notation for the approximate MS likelihood as a function of the set of measurements $\mathbf{Z}_k^c$ and the extent state X_k. The particle filter proceeds to approximate the posterior at time k by a new set of weighted particles

$$\left\{ w_k^{(i)}, X_k^{(i)} \right\}_{i=1}^{N_p} \tag{37}$$

as described in Algorithm 1.

Particles are sampled from the importance distribution

$$q\left(\cdot | X_{k-1}^{(i)}, \mathbf{Z}_k^c\right) = \phi^{-1}\left(\phi(X_{k-1}^{(i)}) + \mathbf{v}_k\right) \tag{39}$$

where $\phi(X)$ extracts from a matrix $X \in \mathbb{S}_{++}^2$ the equivalent ellipse's minor axis, major axis, and orientation, and $\phi^{-1}(\cdot)$ is the inverse, i.e., $\phi^{-1}(\cdot)$ generates a matrix $X \in \mathbb{S}_{++}^2$ from

a minor axis, a major axis, and an orientation.[3] The random variable $\mathbf{v}_k$ is zero-mean Gaussian distributed[4] with covariance matrix

$$\Sigma_v = \text{diag}\left((\sigma^p_{ax_{\min}})^2, (\sigma^p_{ax_{\max}})^2, (\sigma^p_\theta)^2\right) \tag{40}$$

where $\sigma^p_{ax_{\min}}$ and $\sigma^p_{ax_{\max}}$ are the standard deviations for the major and minor axes, σ^p_θ is the standard deviation for the orientation, and diag $(\cdot)$ produces a diagonal matrix.

Then, particle weights are updated based on the likelihood function of the observed data $\mathbf{Z}^c_k$ from all sensors, see (38). The likelihood $\mathcal{L}_k\left(\mathbf{Z}^c_k|X_k\right)$ is given in (36), and takes into account all information at time k. Last, a resampling strategy is adopted to avoid particle degeneracy problem, e.g., see [37].

A target extent estimate is given by the *minimum mean square error* estimator, which is optimal in terms of MSE

$$\hat{X}_{k|k} \triangleq E\left[X_k|\mathbf{Z}^{c,k}\right] = \int X_k \; p\left(X_k|\mathbf{Z}^{c,k}\right) dX_k \tag{41}$$

$$\approx \sum_{i=1}^{N_p} X^{(i)}_k w^{(i)}_k \tag{42}$$

where the approximation is given by the particle representation and N_p is the number of particles. Afterward, the estimation at time k, i.e., $\hat{X}_k$, is used for the next prediction step.

IV. EXTENDED TARGET PREDICTION

In tracking algorithms, the update is typically coupled with a prediction. The same prediction can be used regardless of the number of sensors. For completeness, the extended target prediction is briefly reviewed here [34].

A. Kinematic State Prediction

The kinematic state transition density is

$$p(\mathbf{x}_k|\mathbf{x}_{k-1}) = \mathcal{N}\left(\mathbf{x}_k \,;\, f_{k,k-1}\left(\mathbf{x}_{k-1}\right), Q_k\right) \tag{43}$$

where $f_{k,k-1}(\mathbf{x}_{k-1})$ is a function that describes the motion of the target. The updated mean and covariance are given by the extended Kalman filter prediction

$$m_{k|k-1} = f_{k,k-1}(\mathbf{x}_{k-1}) \tag{44}$$

$$P_{k|k-1} = F_{k,k-1} P_{k-1|k-1} F^{\mathrm{T}}_{k,k-1} + Q_k \tag{45}$$

where

$$F_{k,k-1} = \nabla_{\mathbf{x}_{k-1}} f_{k,k-1}(\mathbf{x}_{k-1})\big|_{\mathbf{x}_{k-1}=\hat{\mathbf{x}}_{k-1|k-1}} \tag{46}$$

is the Jacobian of $f_{k,k-1}(\mathbf{x}_{k-1})$ with respect to the state $\mathbf{x}_{k-1}$, evaluated at the expected value $\hat{\mathbf{x}}_{k-1|k-1}$, and Q_k is the process noise covariance.

B. Inverse Wishart Extent Prediction

In case the extent pdf is approximated by an inverse Wishart pdf, the extent state transition density is

$$p(X_k|X_{k-1}, \mathbf{x}_{k-1}) = \mathcal{W}_d\left(X_k \,;\, \nu_{k|k-1}, \frac{\Phi(\mathbf{x}_{k-1}) X_{k-1} \Phi(\mathbf{x}_{k-1})^{\mathrm{T}}}{\nu_{k|k-1}}\right) \tag{47}$$

where $\Phi(\cdot)$ is a rotation matrix and the Wishart pdf is defined as in Table I. Given the posterior extent X_{k-1} and the posterior kinematic state $\mathbf{x}_{k-1}$, the expected predicted extent is $\Phi(\mathbf{x}_{k-1}) X_{k-1} \Phi(\mathbf{x}_{k-1})^{\mathrm{T}}$. The parameter $\nu_{k|k-1}$ governs the extent process noise: The larger the $\nu_{k|k-1}$, the lower the process noise. Thus, the extent prediction corresponds to rotating the extent by an amount specified by the kinematic state, and increasing the covariance. In [34], the predicted parameters $v_{k|k-1}$ and $V_{k|k-1}$ are computed using a series of density approximations that minimize the Kullback–Leibler divergence. Here, we use a computationally efficient approximation and update the parameters as follows:

$$v_{k|k-1} = 2d + 2 + e^{-T_s/\tau}\left(v_{k-1|k-1} - 2d - 2\right) \tag{48}$$

$$V_{k|k-1} = \left(v_{k|k-1} - 2d - 2\right) \times \frac{\Phi(\hat{\mathbf{x}}_{k-1|k-1}) V_{k-1|k-1} \Phi(\hat{\mathbf{x}}_{k-1|k-1})}{v_{k-1|k-1} - 2d - 2} \tag{49}$$

where τ is a time constant related to the agility with which the target may change its extent over time, T_s is the sampling time, and d is the dimension of the extent matrix. Thus, in this approximate prediction the parameter τ replaces the Wishart transition density degrees of freedom $\nu_{k|k-1}$. However, note that the effect of the prediction is the same as if the prediction from [34] had been used: The extent expected value is rotated, and the covariance is increased.

C. Particle Approximation Extent Prediction

Given the hypothesis that the extent does not tend to change over time, inspired by [9], we exploit as extent prediction

$$\hat{X}_{k|k-1} = \hat{X}_{k-1|k-1} \tag{50}$$

where $\hat{X}_{k-1|k-1}$ is given by the estimator in (42) at time $k-1$ and $\hat{X}_{k|k-1}$ is the extent prediction at time k.

V. NUMERICAL SIMULATION STUDY

The presented Bayesian ETT updates are compared using simulated data.

[3] Note that it is theoretically possible that $\phi(X^{(i)}_{k-1}) + \mathbf{v}_k$ gives a length or a width that is not positive; a zero or negative length/width does not have a physical interpretation. In practice, this unlikely issue has a simple solution: if the length/width is smaller than $e_{\min}$, it is set equal to $e_{\min}$.

[4] Other importance sampling distributions can be used, e.g., direct sampling of random matrices. The advantage of the proposed importance distribution is the simplicity in setting its parameters, thanks to their physical meaning (e.g., for ship tracking they represent the length, width, and orientation of ships). For importance sampling, the inverse Wishart pdf was tested, and similar performance was seen in this case. Using a Gaussian pdf in the importance sampling is preferred because the Gaussian pdf has more flexibility in setting the "randomness" of the three parameters that determine the shape and size of the target extent, i.e., the orientation and the two axes.

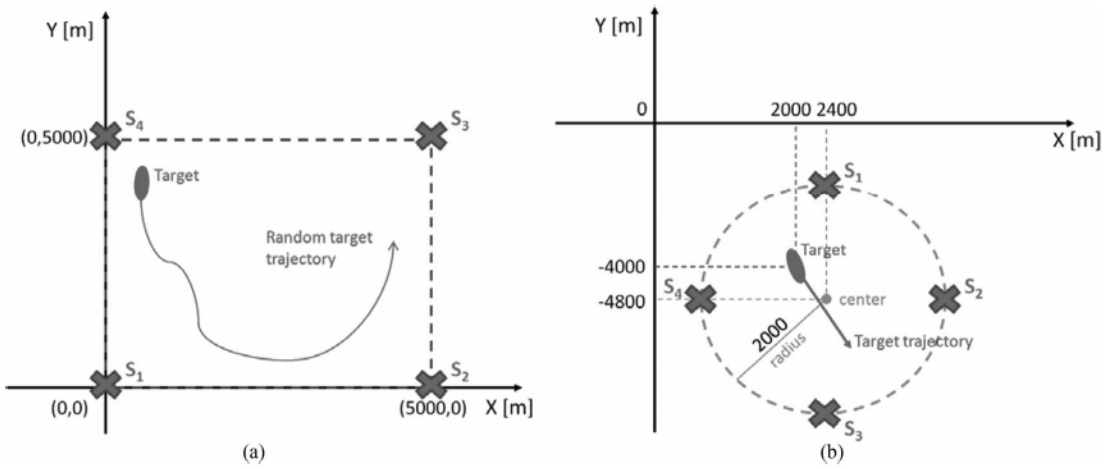

Fig. 1. Two simulators are depicted: (a) Simulator 1 and (b) Simulator 2.

TABLE II
Parameter Setting Simulator 1

Parameter	Notation	Value
Sampling time	T_s	1 s
Std. process noise	σ_{pos}	0.1 m·s^{-2}
Maximum turn-rate	$\theta_{\max}$	1°
Std. turn-rate noise	σ_{ϕ}	0.1°
Std. heading noise	σ_h	1°
Target length	l_t	70 m
Target width	w_t	15 m
Number of frames	$k_{\max}$	200
Maximum velocity target	$v_{\max}$	15 m ·s^{-1}
Minimum velocity target	$v_{\min}$	0.5 m ·s^{-1}
Num. detects. time per sensor	N_d	variable
Num. of sensors	S	4
Std. noise range	σ_r	10 m
Std. noise azimuth	σ_{θ}	2°

TABLE III
Parameter Setting Simulator 2

Parameter	Notation	Value
Sampling time	T_s	1 s
Std. process noise	σ_{pos}	10^{-8} m·s^{-2}
Target length	l_t	100 m
Target width	w_t	30 m
Target orientation	ϕ_t	$\pi/4$
Num. of frames	$k_{\max}$	200
Num. detects. time per sensor	N_d	20–1000
Num. of sensors	S	1 – 10
Std. noise range	σ_r	1–20 m
Std. noise azimuth	σ_{θ}	1°–5°

TABLE IV
Parameter Setting Algorithms for Simulator 1

Parameter	Notation	Value
Sampling time	T_s	1 s
Std. process noise	σ_{pos}	0.1 m·s^{-2}
Time constant	τ	10
Scaling factor	ρ	1
Num. of particles	Np	10^3
Std. prediction axis min.	$\sigma^p_{ax_{\min}}$	1 m
Std. prediction axis max.	$\sigma^p_{ax_{\max}}$	2 m
Std. prediction orientation	σ^p_{θ}	2°

TABLE V
Parameter Setting Algorithms for Simulator 2

Parameter	Notation	Value
Sampling time	T_s	1 s
Std. process noise	σ_{pos}	10^{-8} m·s^{-2}
Time constant	τ	10
Scaling factor	ρ	1
Num. of particles	Np	10^3
Std. prediction axis min.	$\sigma^p_{ax_{\min}}$	0.6 m
Std. prediction axis max.	$\sigma^p_{ax_{\max}}$	0.6 m
Std. prediction orientation	σ^p_{θ}	0.3°

A. Setup

The simulator setups are shown in Fig. 1. The first simulator, called Simulator 1 from here on, consists of four sensors, see Fig. 1(a). In each Monte Carlo run, the target's initial position is randomly selected within the sensor network's hull, and the target tracks are randomly generated. The simulated target follows both linear and curved trajectories. The number of detections per scan is variable and depends on the distance between the target and the sensor, as well as on the simulator's parameters, i.e., the azimuthal accuracy and the range resolution. The parameters are summarized in Table II. The goal of this simulator is to obtain the average performance of the different updates when Monte Carlo trials are performed.

The second simulator, called Simulator 2 from here on, consists of a variable number of sensors (ranging from 1 to 10) equally spaced on a circumference of radius 2 km and center 2.4 km in x and -4.8 km in y, see Fig. 1(b). In this case, the target moves on a straight line and has a fixed starting point. The simulation environment is fixed and detailed analysis, such as varying number of sensors or sensor noises, can be safely performed. The Simulator 2 parameters are summarized in Table III.

Finally, Tables IV and V show the basic sets of parameters used by the compared approaches when Simulators 1 and 2 are exploited, respectively.

The random vector $\mathbf{x}_k = [\mathbf{p}_k,\ \mathbf{v}_k,\ \omega_k]^{\mathrm{T}} \in \mathbb{R}^5$ is the kinematic state, and describes target's position $\mathbf{p}_k \in \mathbb{R}^2$, velocity

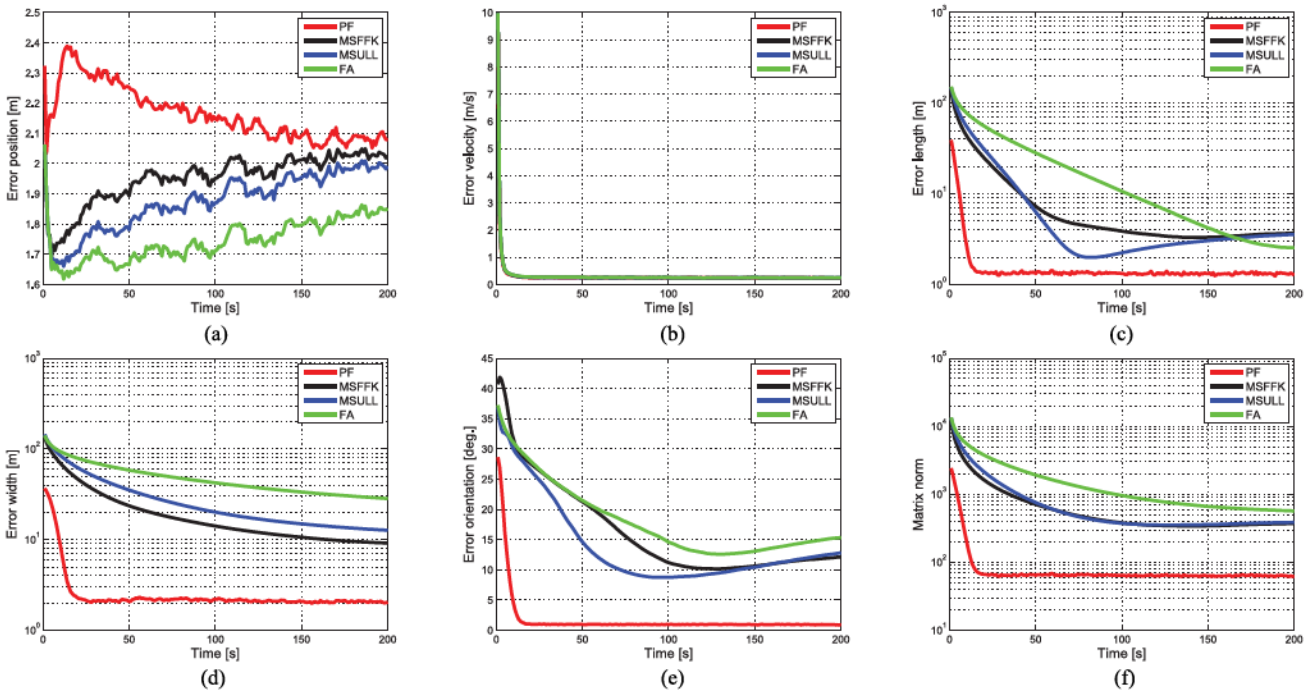

Fig. 2. Errors in (a) position, (b) velocity, (c) length, (d) width, (e) orientation, and the (f) Frobenius matrix error are depicted for the four compared approaches averaged on 10^3 Monte Carlo trials on Simulator 1.

$\mathbf{v}_k \in \mathbb{R}^2$ and turn-rate $\omega_k \in \mathbb{R}^1$. The motion model $\mathbf{f}(\cdot)$ and process noise covariance $\mathbf{Q}$ are

$$\mathbf{f}(X_k) = \begin{bmatrix} 1 & 0 & \frac{\sin(\omega_k T_s)}{\omega_k} & \frac{-1+\cos(\omega_k T_s)}{\omega_k} & 0 \\ 0 & 1 & \frac{1-\cos(\omega_k T_s)}{\omega_k} & \frac{\sin(\omega_k T_s)}{\omega_k} & 0 \\ 0 & 0 & \cos(\omega_k T_s) & -\sin(\omega_k T_s) & 0 \\ 0 & 0 & \sin(\omega_k T_s) & \cos(\omega_k T_s) & 0 \\ 0 & 0 & 0 & 0 & 1 \end{bmatrix} X_k, \tag{51a}$$

$$\mathbf{Q} = \mathbf{G}\,\mathrm{diag}\left(\left[\sigma_a^2\,,\ \sigma_a^2\,,\ \sigma_\omega^2\right]\right)\mathbf{G}^{\mathrm{T}},\quad \mathbf{G} = \begin{bmatrix} \frac{T_s^2}{2}\mathbf{I}_2 & \mathbf{0}_{2\times 1} \\ T_s\mathbf{I}_2 & \mathbf{0}_{2\times 1} \\ \mathbf{0}_{1\times 2} & T_s \end{bmatrix} \tag{51b}$$

where T_s is the sampling time, σ_a is the acceleration standard deviation, and σ_ω is the turn-rate standard deviation. The rotation matrix $\Phi(\cdot)$ is defined as

$$\Phi(X_k) = \begin{bmatrix} \cos(\omega_k T_s) & -\sin(\omega_k T_s) \\ \sin(\omega_k T_s) & \cos(\omega_k T_s) \end{bmatrix}. \tag{52}$$

The performance metrics used for the assessment are the root mean square errors in position (ϵ^{pos}), velocity (ϵ^{vel}), length (ϵ^{len}), width (ϵ^{wid}), and orientation (ϵ^{or}). Furthermore, the Frobenius matrix error (ϵ^{FE}) for the target extent X_k is adopted to have an overall performance index for target's extent estimation.

TABLE VI
Estimation Errors Averaged on 10^3 Monte Carlo Trials on Simulator 1

Algorithm	ϵ^{pos} [m]	ϵ^{vel} [m·s^{-1}]	ϵ^{wid} [m]	ϵ^{len} [m]	ϵ^{or} [°]	ϵ^{FE}
FA	**1.75**	0.328	49.1	21.3	18.1	1698.7
MSULL	1.88	0.324	30.0	10.9	14.0	969.3
MSFFK	1.95	0.324	22.2	10.3	16.3	830.1
PF	2.17	**0.317**	**3.2**	**2.0**	**1.72**	**110.9**

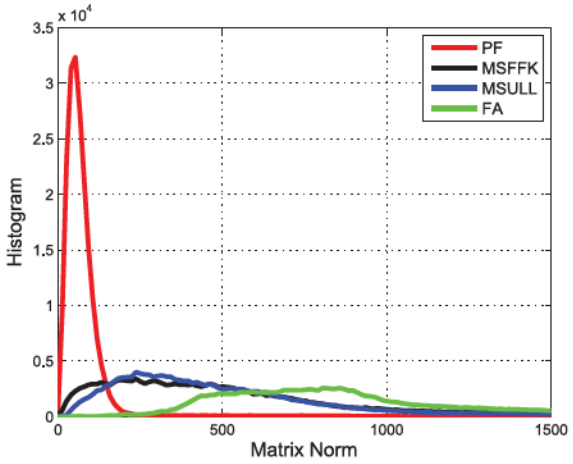

Fig. 3. Histogram of the Frobenius matrix errors for the four compared approaches averaged on 10^3 Monte Carlo trials on Simulator 1.

B. Results

Simulator 1: Fig. 2 shows the results averaged over 10^3 Monte Carlo trials. The PF clearly has the smallest extent estimation errors; however, the price for the improved performance is an increase in the computational burden.

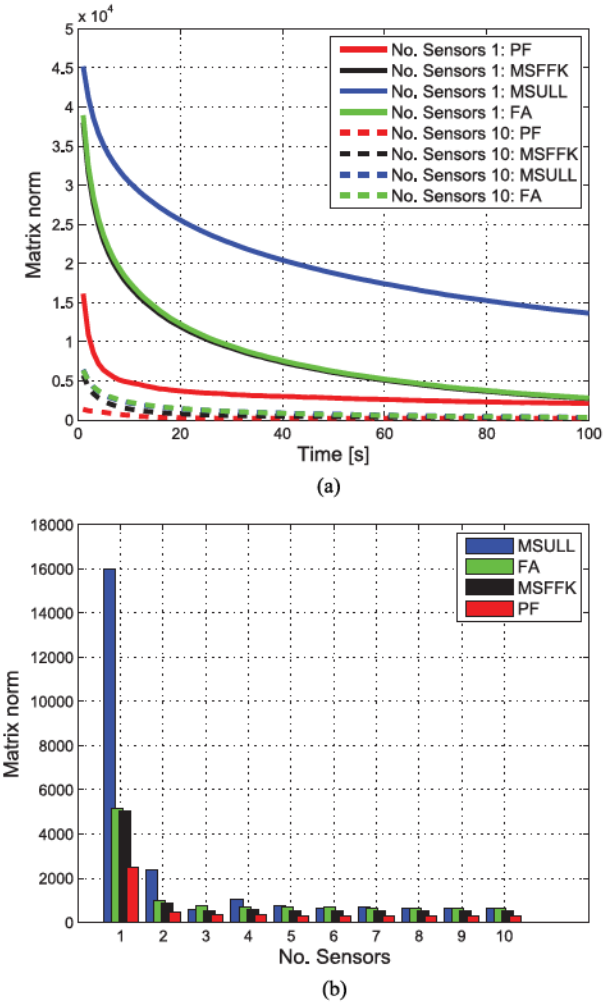

Fig. 4. Frobenius matrix error versus the number of the sensors is depicted for the four compared approaches: (a) time behavior and (b) histogram representation. The results are averaged on 10^3 Monte Carlo trials using Simulator 2.

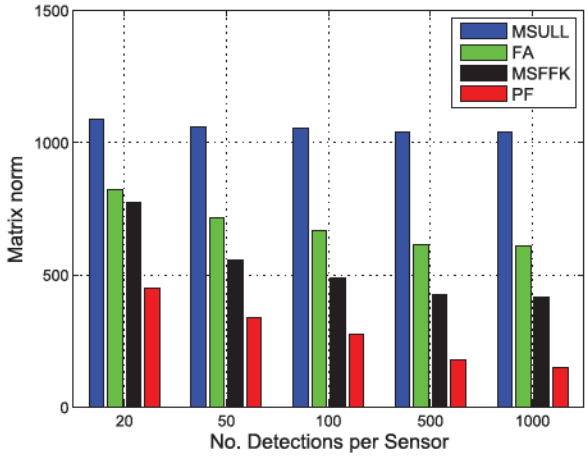

Fig. 5. Histogram representation of the Frobenius matrix error versus the number of detections per sensor is depicted. The results are averaged on 10^3 Monte Carlo trials using Simulator 2.

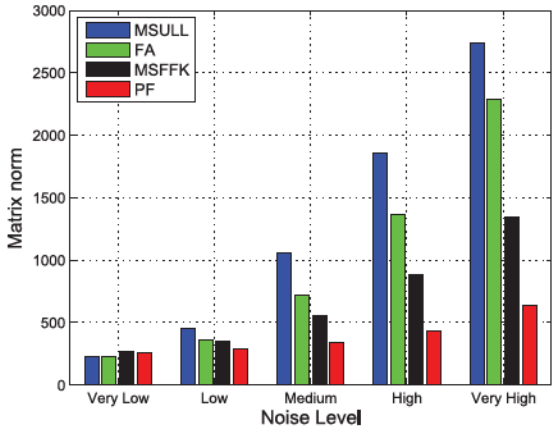

Fig. 6. Histogram representation of the Frobenius matrix error versus the sensor noise level is depicted. The results are averaged on 500 Monte Carlo trials using Simulator 2. "Very low" indicates $\sigma_r = 1$ m and $\sigma_\theta = 1°$, "low" indicates $\sigma_r = 5$ m and $\sigma_\theta = 2°$, "medium" indicates $\sigma_r = 15$ m and $\sigma_\theta = 3°$, "high" indicates $\sigma_r = 20$ m and $\sigma_\theta = 4°$, and "very high" indicates $\sigma_r = 20$ m and $\sigma_\theta = 5°$.

How the computational time scales with the number of particles is shown in Fig. 7. One can note that the kinematics (i.e., position and velocity) are well estimated by all four updates. Very small differences can be seen for the position estimates; however, these are limited to less than 1 m.

Regarding the estimated extent, the errors for length, width, and orientation follow the same trend as the Frobenius matrix error does. FA is the worst algorithm, whereas MSULL and MSFFK have comparable average performance. Table VI summarizes the estimation errors (the best outcomes are highlighted in boldface text). Fig. 3 provides empirical distributions of the Frobenius matrix errors for the four updates, confirming the above-mentioned analysis and ranking of the updates.

Simulator 2: The other test cases are run using Simulator 2. From here on, the kinematic estimations will be omitted because the four algorithms share the kinematic measurement update step and same performance are expected for these parameters. Furthermore, only the Frobenius matrix error, which is the unique overall quality index, will be considered to point out the differences in the targets' extent estimation.

As first analysis, the variation of number of sensors is considered. Fig. 4 shows the behavior of the Frobenius matrix error over time and the related histogram representation. The higher the number of sensors to fuse, the greater the accuracy of all the tracking approaches. A final remark is related to the ranking among the algorithms, which is quite independent from the number of sensors.

The same considerations can be done when the Frobenius matrix error versus the number of target detections per sensor is evaluated, see Fig. 5. The higher the number of target detections per sensor, the greater the performance accuracy (measured by the Frobenius matrix error).

A further analysis is devoted to the robustness of the compared approaches with respect to the sensor noise level. Five levels of noises are exploited in Fig. 6 ranging from "very low" to "very high." Obviously, the improvements in

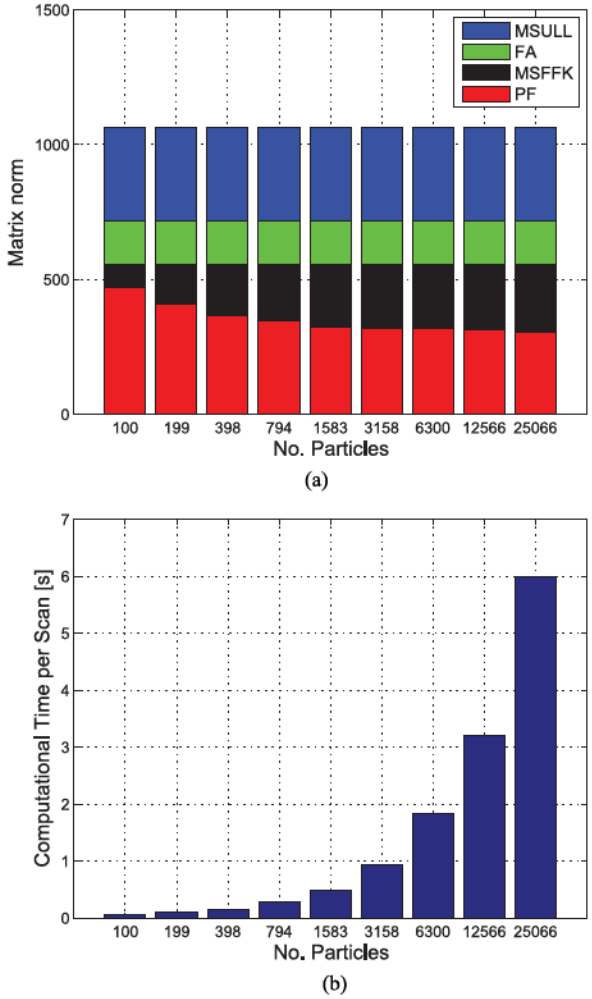

Fig. 7. Histogram representation of the Frobenius matrix error versus the number of particles is depicted in (a), whereas the computational time per scan versus the number of particles for the PF approach is shown in (b) using Simulator 2.

the algorithm performance are clear when an increase of the sensor noise is shown. In the case of low sensor noise levels, the performance of MSFFK, MSULL, FA, and PF are comparable. On other hand, when the sensor noise level can be considered high, the ranking among the compared algorithms is better defined. The best approach is always represented by the PF method, whereas MSFFK shows its ability to deal with high levels of sensor noise.

Finally, an analysis varying the number of particles used by the PF approach is depicted in Fig. 7. It is clear that about 10^3 particles seem to be enough: Fewer means noticeably poorer error, while more particles seem to contribute little compared to the increase of the computational burden. Thus, a number of particles of 10^3 (used in this paper for both the setups) can be advisable.

VI. CONCLUSION AND FUTURE DEVELOPMENTS

In this paper, a study of MS Bayesian ETT has been shown. The extended targets have been modeled into the random matrix framework, i.e., the extended target state consists of a kinematic state vector and an extent matrix. Four different extent matrix measurement updates have been presented using the same MS kinematic vector measurement update. One of the updates is based on a particle approximation of the extent state pdf; the other three are based on an inverse Wishart representation of the extent state pdf. Of the inverse Wishart updates, one is based on FAs, and the last two are MS generalizations of existing SS updates.

Extensive numerical results, using two different simulation setups, pointed out that the best performance is obtained by the PF-based approach. As usual, there is no free lunch, and the improved performance comes at the price of an increased computational burden.

Finally, the integration of the MS filters proposed in this paper into a multiple ETT algorithm, enabling to work in a real environment with clutter measurements and multiple extended targets, deserves further investigations.

APPENDIX
A. REVIEW OF SS UPDATE

In this section, we give a brief review of SS GIW updates, focusing on two different updates that are later generalized to multiple sensors, namely, the updates found in [9] and [35]. With $S = 1$ sensor, the MS measurement likelihood (14) simplifies to

$$p\left(\mathbf{Z}_k^1 \,|\mathbf{x}_k, X_k, n_k^1\right) = \prod_{j=1}^{n_k^1} \mathcal{N}\left(\mathbf{z}_k^{1,j};\, H_k\mathbf{x}_k, \rho X_k + R_k^1\right). \tag{53}$$

A. Gaussian Kinematic State Update

The SS kinematic state update used in [9] and [35] updates the Gaussian parameters as

$$m_{k|k}^{\mathrm{SS}} = m_{k|k-1} + K_{k|k-1}^1\left(\bar{\mathbf{z}}_k^1 - H_k m_{k|k-1}\right) \tag{54}$$

$$P_{k|k}^{\mathrm{SS}} = P_{k|k-1} - K_{k|k-1}^1 H_k P_{k|k-1} \tag{55}$$

where

$$S_{k|k-1}^1 = H_k P_{k|k-1} H_k^{\mathrm{T}} + \hat{Y}_{k|k-1}^1 \tag{56}$$

$$K_{k|k-1}^1 = P_{k|k-1} H_k^{\mathrm{T}}\left(S_{k|k-1}^1\right)^{-1} \tag{57}$$

and $\bar{\mathbf{z}}_k^1$ and $\hat{Y}_{k|k-1}^1$ are defined in Table I for $s = 1$.

B. Inverse Wishart Extent Update

1) *FFK:* The SS extent update in [9] is based on the assumption that the extent X_k is approximately equal to the predicted estimate $\hat{X}_{k|k-1}$. This update is here called FFK, after the authors' initials. The inverse Wishart parameters are updated as

$$v_{k|k}^{\mathrm{FFK}} = v_{k|k-1} + n_k \tag{58}$$

$$V_{k|k}^{\mathrm{FFK}} = V_{k|k-1} + Z_{k|k-1}^1 + L_{k|k-1}^1 \tag{59}$$

where

$$Z^1_{k|k-1} = \hat{X}^{\frac{\mathrm{T}}{2}}_{k|k-1} \left(\hat{Y}^1_{k|k-1}\right)^{-\frac{\mathrm{T}}{2}} Z^1_k \left(\hat{Y}^1_{k|k-1}\right)^{-\frac{1}{2}} \hat{X}^{\frac{1}{2}}_{k|k-1} \quad (60)$$

$$L^1_{k|k-1} = \hat{X}^{\frac{\mathrm{T}}{2}}_{k|k-1} \left(S^1_{k|k-1}\right)^{-\frac{\mathrm{T}}{2}} N^1_{k|k-1} \left(S^1_{k|k-1}\right)^{-\frac{1}{2}} \hat{X}^{\frac{1}{2}}_{k|k-1} \quad (61)$$

$$N^1_{k|k-1} = \left(\bar{\mathbf{z}}^1_{k|k-1} - H_k m_{k|k-1}\right)\left(\bar{\mathbf{z}}^1_{k|k-1} - H_k m_{k|k-1}\right)^{\mathrm{T}} \quad (62)$$

and $\bar{\mathbf{z}}^1_k$, $\hat{X}_{k|k-1}$, and $\hat{Y}^1_{k|k-1}$ are defined in Table I.

2) *ULL:* The SS update in [35] is derived using linearization of the logarithm of the likelihood (14) around the nominal point

$$(\mathbf{x}_k, X_k) = \left(\hat{\mathbf{x}}_{k|k-1}, \hat{X}_{k|k-1}\right) \quad (63)$$

followed by bias compensation. This update is here called ULL (unbiased log-likelihood linearization). Derivation details are given in [35], where a small simulation study shows that the ULL update outperforms the FFK update. The inverse Wishart parameters are updates as

$$v^{\mathrm{ULL}}_{k|k} = v_{k|k-1} + n^1_k \quad (64)$$

$$V^{\mathrm{ULL}}_{k|k} = V_{k|k-1} + M^1_{k|k-1} \quad (65)$$

where

$$M^1_{k|k-1} = n^1_k \hat{X}_{k|k-1} + n^1_k \rho \hat{X}_{k|k-1} (C^1_{k|k-1})^{-1} \times \left(\Psi^1_{k|k-1} - C^1_{k|k-1}\right)(C^1_{k|k-1})^{-1} \hat{X}_{k|k-1} \quad (66)$$

$$\Psi^1_{k|k-1} = \frac{1}{n^1_k} \sum_{j=1}^{n^1_k} \left(\mathbf{z}^{1,j}_k - H_k m_{k|k-1}\right)\left(\mathbf{z}^{1,j}_k - H_k m_{k|k-1}\right)^{\mathrm{T}} \quad (67)$$

$$= \left(\bar{\mathbf{z}}^1_k - H_k m_{k|k-1}\right)\left(\bar{\mathbf{z}}^1_k - H_k m_{k|k-1}\right)^{\mathrm{T}} + \frac{Z^1_k}{n^1_k} \quad (68)$$

$$C^1_{k|k-1} = H_k P_{k|k-1} H^{\mathrm{T}}_k + \rho \hat{X}_{k|k-1} + R^1_k \quad (69)$$

and $\hat{X}_{k|k-1}$ is defined in Table I.

B. DERIVATION SKETCH

In this section, we give some details related to the derivation of the MS generalization of the FFK and the ULL updates (i.e., MSFFK and MSULL).

A. MSFFK

The MS likelihood can be written as

$$p(\mathbf{Z}^c_k|\mathbf{x}_k, X_k) = \prod_{s=1}^{S} \prod_{j=1}^{n^s_k} \mathcal{N}\left(\mathbf{z}^{s,j}_k ; H_k\mathbf{x}_k, \rho X_k + R^s_k\right). \quad (70)$$

The product for the generic sensor s in (70), i.e., the SS likelihood, can be factorized as follows:

$$p(\mathbf{Z}^c_k|\mathbf{x}_k, X_k) \propto \prod_{s=1}^{S} \mathcal{N}\left(\bar{\mathbf{z}}^s_k ; H_k\mathbf{x}_k, \frac{\rho X_k + R^s_k}{n^s_k}\right) \times \prod_{s=1}^{S} |\rho X_k + R^s_k|^{-\frac{n^s_k - 1}{2}} \operatorname{etr}\left(-\frac{1}{2} Z^s_k \left(\rho X_k + R^s_k\right)^{-1}\right). \quad (71)$$

see, e.g., [8, Appendix C] or [24, Appendix A].

By applying the Gaussian product formula, and using the approximation in (26), we get

$$p(\mathbf{Z}^c_k|\mathbf{x}_k, X_k) \propto \mathcal{N}\left(\bar{\mathbf{z}}^c_{k|k-1} ; H_k\mathbf{x}_k, Y^c_k\right) \times \prod_{s=1}^{S} |X_k|^{-\frac{n^s_k - 1}{2}} \operatorname{etr}\left(-\frac{1}{2} Z^s_{k|k-1} X^{-1}_k\right) \quad (72)$$

with $Z^s_{k|k-1}$ defined in (23c) and

$$Y^c_k = \left[\sum_{s=1}^{S} \left(\frac{\rho X_k + R^s_k}{n^s_k}\right)^{-1}\right]^{-1} \quad (73)$$

Multiplying with a factorized prior, we get

$$p\left(\mathbf{x}_k, X_k|\mathbf{Z}^{c,k}\right) \propto p\left(\mathbf{Z}^c_k|\mathbf{x}_k, X_k\right) p\left(\mathbf{x}_k, X_k|\mathbf{Z}^{c,k-1}\right)$$

$$\propto p\left(\mathbf{Z}^c_k|\mathbf{x}_k, X_k\right) p\left(\mathbf{x}_k|\mathbf{Z}^{c,k-1}\right) p\left(X_k|\mathbf{Z}^{c,k-1}\right) \quad (74)$$

$$\propto \mathcal{N}\left(\mathbf{x}_k ; m^{MS}_{k|k}, P^{MS}_{k|k-1}\right) \mathcal{N}\left(\bar{\mathbf{z}}^c_{k|k-1} ; H_k m_{k|k-1}, S^c_{k|k-1}\right) \times |X_k|^{-\frac{n_k - S}{2}} \prod_{s=1}^{S} \operatorname{etr}\left(-\frac{1}{2} Z^s_{k|k-1} X^{-1}_k\right) \times \mathcal{IW}_d\left(X_k ; v_{k|k-1}, V_{k|k-1}\right). \quad (75)$$

By applying a Cholesky approximation of the type (26) to $S^c_{k|k-1}$, the posterior becomes

$$p(\mathbf{x}_k|\mathbf{Z}^{c,k-1}) p(X_k|\mathbf{Z}^{c,k-1})$$

$$\propto \mathcal{N}\left(\mathbf{x}_k ; m^{MS}_{k|k}, P^{MS}_{k|k-1}\right) \operatorname{etr}\left(-\frac{1}{2} L^c_{k|k-1} X^{-1}_k\right) |X_k|^{-\frac{n_k}{2}} \times \operatorname{etr}\left(-\frac{1}{2} \sum_{s=1}^{S} Z^s_{k|k-1} X^{-1}_k\right) \mathcal{IW}_d\left(X_k ; v_{k|k-1}, V_{k|k-1}\right) \quad (76)$$

$$\propto \mathcal{N}\left(\mathbf{x}_k ; m^{MS}_{k|k}, P^{MS}_{k|k-1}\right) \mathcal{IW}_d\left(X_k ; v^{\mathrm{MSFFK}}_{k|k}, V^{\mathrm{MSFFK}}_{k|k}\right). \quad (77)$$

B. MSULL

The MS log likelihood is written as

$$\log\ p(\mathbf{Z}^c_k|\mathbf{x}_k, X_k) = \sum_{s=1}^{S} \sum_{j=1}^{n^s_k} \log \mathcal{N}\left(\mathbf{z}^{s,j}_k ; H_k\mathbf{x}_k, \rho X_k + R^s_k\right) \quad (78)$$

$$\propto \sum_{s=1}^{S} n_k^s \log\det(\rho X_k + R_k^s) \tag{79}$$
$$+ \sum_{j=1}^{n_k^s} \left(\mathbf{z}_k^{s,j} - H_k\mathbf{x}_k\right)^{\mathrm{T}} \left(\rho X_k + R_k^s\right)^{-1} \left(\mathbf{z}_k^{s,j} - H_k\mathbf{x}_k\right)$$
$$= \sum_{s=1}^{S} n_k^s \left[\log\det(X_k) + \log\det(\rho\mathbb{I} + X_k^{-\mathrm{T}/2} R_k^s X_k^{-1/2})\right]$$
$$+ \sum_{j=1}^{n_k^s} \mathrm{Tr}\left[\left(\mathbf{z}_k^{s,j} - H_k\mathbf{x}_k\right)\left(\mathbf{z}_k^{s,j} - H_k\mathbf{x}_k\right)^{\mathrm{T}} \left(\rho X_k + R_k^s\right)^{-1}\right] \tag{80}$$

where $\mathbb{I}$ is the identity matrix and $\mathrm{Tr}[\cdot]$ is the matrix trace. By introducing

$$\Psi_k = X_k^{-1} \tag{81}$$
$$\Phi_k^s = \left(\mathbf{z}_k^{s,j} - H_k\mathbf{x}_k\right)\left(\mathbf{z}_k^{s,j} - H_k\mathbf{x}_k\right)^{\mathrm{T}} \tag{82}$$

Taylor expanding around the point

$$\hat{\Psi}_{k|k-1} = \hat{X}_{k|k-1}^{-1} \tag{83}$$
$$\hat{\Phi}_{k|k-1}^s = \left(\mathbf{z}_k^{s,j} - H_k\hat{\mathbf{x}}_{k|k-1}\right)\left(\mathbf{z}_k^{s,j} - H_k\hat{\mathbf{x}}_{k|k-1}\right)^{\mathrm{T}} \tag{84}$$

and performing a bias compensation, we get

$$p(\mathbf{Z}_k^c|\mathbf{x}_k, X_k) \propto \prod_{s=1}^{S}\prod_{j=1}^{n_k^s} \mathcal{N}\left(\mathbf{z}_k^{s,j}\,;\, H_k\mathbf{x}_k, \rho\hat{X}_{k|k-1} + R_k^s\right)$$
$$\times \prod_{s=1}^{S} \mathcal{IW}_d\left(X_k\,;\, n_k^s, M_{k|k-1}^s\right). \tag{85}$$

See [35] for a proof in the case of a SS. The MS generalization is straightforward due to the independence between the sensors. The double-product of Gaussians can be rewritten as

$$\mathcal{N}\left(\bar{\mathbf{z}}_{k|k-1}^c\,;\, H_k\mathbf{x}_k, Y_{k|k-1}^c\right). \tag{86}$$

Its proof follows from [24, App. A] and applying the Gaussian product formula.

By multiplying the likelihood with a factorized prior, the MSULL kinematic update follows from the standard Kalman filter update. The product of inverse Wishart likelihoods and the inverse Wishart prior distribution can easily be rewritten to obtain the MSULL extent update (24a) and (24b).

REFERENCES

[1] Y. Bar-Shalom, P. Willett, and X. Tian
Tracking and Data Fusion: A Handbook of Algorithms. Storrs, CT, USA: YBS Publishing, Apr. 2011.

[2] R. Mahler
Multitarget Bayes filtering via first-order multitarget moments
IEEE Trans. Aerosp. Electron. Syst., vol. 39, no. 4, pp. 1152–1178, Oct. 2003.

[3] S. S. Blackman
Multiple hypothesis tracking for multiple target tracking
IEEE Aerosp. Electron. Syst. Mag., vol. 19, no. 1, pp. 5–18, Jan. 2004.

[4] G. Vivone, P. Braca, and J. Horstmann
Knowledge-based multi-target ship tracking for HF surface wave radar systems
IEEE Trans. Geosci. Remote Sens., vol. 53, no. 7, pp. 3931–3949, Jul. 2015.

[5] K. Granström, M. Baum, and S. Reuter
Extended object tracking: Introduction, overview and applications
J. Adv. Inform. Fusion, vol. 12, no. 2, Dec. 2017.

[6] K. Gilholm and D. Salmond
Spatial distribution model for tracking extended objects
IEE Proc. Radar, Sonar Navig., vol. 152, no. 5, pp. 364–371, Oct. 2005.

[7] K. Gilholm, S. Godsill, S. Maskell, and D. Salmond
Poisson models for extended target and group tracking
In *Proc. SPIE Conf. Signal Proc. Small Targ.*, San Diego, CA, USA, Aug. 2005, pp. 230–241.

[8] J. W. Koch
Bayesian approach to extended object and cluster tracking using random matrices
IEEE Trans. Aerosp. Electron. Syst., vol. 44, no. 3, pp. 1042–1059, Apr. 2008.

[9] M. Feldmann, D. Franken, and J. W. Koch
Tracking of extended objects and group targets using random matrices
IEEE Trans. Signal Process., vol. 59, no. 4, pp. 1409–1420, Apr. 2011.

[10] M. Baum and U. D. Hanebeck
Extended object tracking with random hypersurface models
IEEE Trans. Aerosp. Electronic Syst., vol. 50, no. 1, pp. 149–159, Jan. 2014.

[11] N. Wahlström and E. Özkan
Extended target tracking using Gaussian processes
IEEE Trans. Signal Process., vol. 63, no. 16, pp. 4165–4178, Aug. 2015.

[12] T. Hirscher, A. Scheel, S. Reuter, and K. Dietmayer
Multiple extended object tracking using Gaussian processes
In *Proc. Int. Conf. Inform. Fusion*, Jul. 2016, pp. 868–875.

[13] E. Özkan, N. Wahlström, and S. J. Godsill
Rao-Blackwellised particle filter for star-convex extended target tracking models
In *Proc. Int. Conf. Inform. Fusion*, Jul. 2016, pp. 1193–1199.

[14] U. Orguner
A variational measurement update for extended target tracking with random matrices
IEEE Trans. Signal Process., vol. 60, no. 7, pp. 3827–3834, Jul. 2012.

[15] K. Granström and O. Orguner
New prediction for extended targets with random matrices
IEEE Trans. Aerosp. Electronic Syst., vol. 50, no. 2, pp. 1577–1589, Apr. 2014.

[16] J. W. Koch and M. Feldmann
Cluster tracking under kinematical constraints using random matrices
Robot. Auton. Syst., vol. 57, no. 3, pp. 296–309, Mar. 2009.

[17] J. Lan and X. R. Li
Tracking of maneuvering non-ellipsoidal extended object or target group using random matrix
IEEE Trans. Signal Proc., vol. 62, no. 9, pp. 2450–2463, May 2014.

[18] K. Granström, P. Willett, and Y. Bar-Shalom
An extended target tracking model with multiple random matrices and unified kinematics
In *Proc. Int. Conf. Inf. Fusion*, Washington, DC, USA, Jul. 2015, pp. 1007–1014.

[19] K. Granström, A. Natale, P. Braca, G. Ludeno, and F. Serafino
Gamma Gaussian inverse Wishart probability hypothesis density for extended target tracking using X-band marine radar data
IEEE Trans. Geosci. Remote Sens., vol. 53, no. 12, pp. 6617–6631, Dec. 2015.

[20] G. Vivone, P. Braca, K. Granström, A. Natale, and J. Chanussot
Converted measurements random matrix approach to extended target tracking using X-band marine radar data
In *Proc. 18th Int. Conf. Inf. Fusion*, Washington, DC, USA, Jul. 2015, pp. 976–983.

[21] G. Vivone, P. Braca, K. Granström, and P. Willett
Multistatic Bayesian extended target tracking
IEEE Trans. Aerosp. Electron. Syst., vol. 52, no. 6, pp. 2626–2643, Dec. 2016.

[22] R. Mahler
PHD filters for nonstandard targets, I: Extended targets
In *Proc. 12th Int. Conf. Inform. Fusion*, Seattle, WA, USA, Jul. 2009, pp. 915–921.

[23] K. Granström, C. Lundquist, and O. Orguner
Extended target tracking using a Gaussian-mixture PHD filter
IEEE Trans. Aerosp. Electronic Syst., vol. 48, no. 4, pp. 3268–3286, Oct. 2012.

[24] K. Granström and U. Orguner
A PHD filter for tracking multiple extended targets using random matrices
IEEE Trans. Signal Process., vol. 60, no. 11, pp. 5657–5671, Nov. 2012.

[25] C. Lundquist, K. Granström, and U. Orguner
An extended target CPHD filter and a Gamma Gaussian inverse Wishart implementation
IEEE J. Sel. Topics Signal Process., vol. 7, no. 3, pp. 472–483, Jun. 2013.

[26] M. Beard, S. Reuter, K. Granström, B.-T. Vo, B.-N. Vo, and A. Scheel
A generalised labelled multi-bernoulli filter for extended multi-target tracking
In *Proc. Int. Conf. Inf. Fusion*, Washington, DC, USA, Jul. 2015, pp. 991–998.

[27] M. Beard, S. Reuter, K. Granström, B.-T. Vo, B.-N. Vo, and A. Scheel
Multiple extended target tracking with labelled random finite sets
IEEE Trans. Signal Process., vol. 64, no. 7, pp. 1638–1653, Apr. 2016.

[28] K. Granström, M. Fatemi, and L. Svensson
Gamma Gaussian inverse-Wishart Poisson multi-Bernoulli filter for extended target tracking
In *Proc. Int. Conf. Inform. Fusion*, Heidelberg, Germany, Jul. 2016, pp. 893–900.

[29] M. Wieneke and J. W. Koch
Probabilistic tracking of multiple extended targets using random matrices
Proc. SPIE, vol. 7698, Apr. 2010, Art. no. 769812.

[30] M. Wieneke and J. W. Koch
A PMHT approach for extended objects and object groups
IEEE Trans. Aerospace Electr. Systems, vol. 48, no. 3, pp. 2349–2370, Jul. 2012.

[31] G. Vivone, P. Granström, K. Braca, and P. Willett
Multiple sensor Bayesian extended target tracking fusion approaches using random matrices
In *Proc. 19th Intern. Conf. Inf. Fusion*, Jul. 2016, pp. 886–892.

[32] A. K. Gupta and D. K. Nagar
Matrix Variate Distributions (ser. Chapman & Hall/CRC Monographs and Surveys in Pure and Applied Mathematics). London, U.K: Chapman & Hall, 2000.

[33] K. Granström and U. Orguner
Estimation and maintenance of measurement rates for multiple extended target tracking
In *Proc. Int. Conf. Inf. Fusion*, Singapore, Jul. 2012, pp. 2170–2176.

[34] K. Granström and U. Orguner
A new prediction update for extended target tracking with random matrices
IEEE Trans. Aerosp. Electron. Syst., vol. 50, no. 2, pp. 1577–1589, Apr. 2014.

[35] T. Ardeshiri, U. Orguner, and F. Gustafsson
Bayesian inference via approximation of log-likelihood for priors in exponential family
2015. arXiv: 1510.01225. [Online]. Available: http://arxiv.org/abs/1510.01225

[36] Q. Gan and C. Harris
Comparison of two measurement fusion methods for Kalman-filter-based multisensor data fusion
IEEE Trans. Aerosp. Electron. Syst., vol. 37, no. 1, pp. 273–279, Jan. 2001.

[37] M. Arulampalam, S. Maskell, N. Gordon, and T. Clapp
A tutorial on particle filters for online nonlinear/non-Gaussian Bayesian tracking
IEEE Trans. Signal Process., vol. 50, no. 2, pp. 174–188, Feb. 2002.

Gemine Vivone received the B.Sc. (*summa cum laude*), M.Sc. (*summa cum laude*), and Ph.D. (highest rank) degrees in information engineering from the University of Salerno, Fisciano, Italy, in 2008, 2011, and 2014, respectively.

He is currently in the Department of Information Engineering, Electrical Engineering and Applied Mathematics, University of Salerno. In 2014, he joined the North Atlantic Treaty Organization (NATO) Science and Technology Organization Centre for Maritime Research and Experimentation, La Spezia, Italy, as a Scientist. In 2013, he was a Visiting Scholar in Grenoble Institute of Technology, Grenoble, France, conducting his research at the Laboratoire Grenoblois de l'Image, de la Parole, du Signal et de l'Automatique GIPSA-Lab. In 2012, he was a Visiting Researcher in the NATO Undersea Research Centre, La Spezia, Italy. His research interests include statistical signal processing, detection of remotely sensed images, data fusion, and tracking algorithms.

Dr. Vivone is a Referee for several journals, such as IEEE TRANSACTIONS ON GEOSCIENCE AND REMOTE SENSING, IEEE JOURNAL OF SELECTED TOPICS IN APPLIED EARTH OBSERVATIONS AND REMOTE SENSING, and IEEE GEOSCIENCE AND REMOTE SENSING LETTERS. He received the Symposium Best Paper Award at the IEEE International Geoscience and Remote Sensing Symposium 2015.

Karl Granström (M'08) received the M.Sc. degree in applied physics and electrical engineering and the Ph.D. degree in automatic control from Linköping University, Linköping, Sweden, in May 2008 and November 2012, respectively. He is currently a Postdoctoral Research Fellow in the Department of Signals and Systems, Chalmers University of Technology, Gothenburg, Sweden. He has previously held postdoctoral positions in the Department of Electrical and Computer Engineering at the University of Connecticut, Storrs, CT, USA, from September 2014 to August 2015, and in the Department of Electrical Engineering, Linköping University from December 2012 to August 2014. His research interests include estimation theory, multiple model estimation, sensor fusion and target tracking, especially for extended targets.

Dr. Granström received paper awards at the Fusion 2011 and Fusion 2012 conferences.

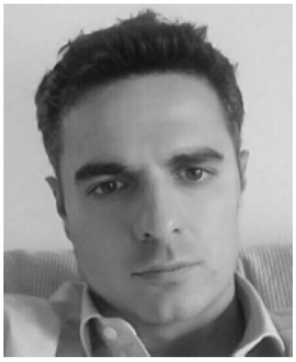

Paolo Braca (M'14–SM'17) received the Laurea (*summa cum laude*) degree in electronic engineering and the Ph.D. degree (highest rank) in information engineering from the University of Salerno, Fisciano, Italy, in 2006 and 2010, respectively.

In 2009, he was a Visiting Scholar in the Department of Electrical and Computer Engineering, University of Connecticut, Storrs, CT, USA. In 2010–2011, he was a Postdoctoral Associate at the University of Salerno. In 2011, he joined the North Atlantic Treaty Organization Science and Technology Organization Centre for Maritime Research and Experimentation, as a Scientist in the Research Department. He is the coauthor of about 100 publications in international scientific journals and conference proceedings. His research interests include statistical signal processing with emphasis on detection and estimation theory, wireless sensor network, multiagent algorithms, target tracking and data fusion, adaptation and learning over graphs, and distributed radar (sonar) processing.

Dr. Paolo Braca was awarded with National Scientific Qualification (Abilitazione Scientifica Nazionale) in 2017, by a qualification committee of professors, selected by the Italian Ministry of Education, Universities and Research, to function as an Associate Professor in Italian Universities. He is an Associate Editor of the IEEE TRANSACTIONS ON SIGNAL PROCESSING, IEEE TRANSACTIONS ON AEROSPACE AND ELECTRONIC SYSTEMS, *ISIF Journal of Advances in Information Fusion*, *EURASIP Journal on Advances in Signal Processing*, and is the Lead Guest Editor of the special issue "Sonar Multi-Sensor Applications and Techniques" in *IET Radar Sonar and Navigation*. From 2014 to 2016, he was an Associate Editor of the IEEE SIGNAL PROCESSING MAGAZINE (E-Newsletter). He is in the Technical Committee of the major international conferences in the field of signal processing and data fusion. He received the Best Student Paper Award (first runner-up) at the 12th International Conference on Information Fusion in 2009.

Peter Willett (F'03) received his B.Sc. degree in engineering science from the University of Toronto in 1982, and the M.E., M.S. and Ph.D. degrees in electrical engineering from Princeton University in 1983, 1984 and 1986, respectively.

He has been a Faculty Member in the Electrical and Computer Engineering Department, University of Connecticut, Storrs, CT, USA, since 1986. Since 1998, he has been a Professor. His research interests include statistical signal processing, detection, machine learning, communications, data fusion, and tracking.

Dr. Willett was the Editor-in-Chief of the IEEE SIGNAL PROCESSING LETTERS (2014–2016), and the Editor-in-Chief of the IEEE TRANSACTIONS ON AEROSPACE AND ELECTRONIC SYSTEMS (2006–2011). He was an AESS Vice President for Publications 2012–2014. From 1998 to 2005, he was an Associate Editor of three active journals, IEEE TRANSACTIONS ON AEROSPACE AND ELECTRONIC SYSTEMS (for Data Fusion and Target Tracking) and IEEE TRANSACTIONS ON SYSTEMS, MAN, AND CYBERNETICS, PARTS A AND B. He is the Associate Editor of the IEEE AEROSPACE AND ELECTRONIC SYSTEMS MAGAZINE. He was a member of the IEEE AESS Board of Governors (2004–2009 and 2010–2016) and of the IEEE Signal Processing Society's Sensor-Array and Multichannel technical committee, and was the Chair in 2015–2016.

Document Data Sheet

Security Classification		Project No.
Document Serial No.	**Date of Issue**	**Total Pages**
CMRE-PR-2019-057	June 2019	15 pp.

Author(s)

Gemine Vivone, Karl Granström, Paolo Braca, Peter Willett

Title

Multiple sensor measurement updates for the extended target tracking random matrix model

Abstract

In this paper, multiple sensor measurement update is studied for a random matrix model. Four different updates are presented and evaluated: three updates based on parametric approximations of the extended target state probability density function and one update based on a Rao-Blackwellized (RB) particle approximation of the state density. An extensive simulation study shows that the RB particle approach shows best performance, at the price of higher computational cost, compared to parametric approximations.

Keywords

Covariance matrices, time measurement, target tracking, noise measurement, density measurement, kinematics, computational modelling

Issuing Organization

NATO Science and Technology Organization
Centre for Maritime Research and Experimentation

Viale San Bartolomeo 400, 19126 La Spezia, Italy

[From N. America:
STO CMRE
Unit 31318, Box 19, APO AE 09613-1318]

Tel: +39 0187 527 361
Fax:+39 0187 527 700

E-mail: library@cmre.nato.int